Bruise chromophore concentrations over time

Mark G. Duckworth[a], Jayme J. Caspall[a], Rudolph L. Mappus IV[a], Linghua Kong[a], Dingrong Yi[b], Stephen H. Sprigle[a]

[a]Center for Assistive Technology and Environmental Access, College of Architecture, Georgia Institute of Technology, 490 Tenth Street, NW, Atlanta, Georgia 30332, U.S.A.
[b]Imaging Research, Sunnybrook Health Sciences Centre & Medical Biophysics Department of University of Toronto, Room S-646, 2075 Bayview Avenue Toronto, ON M4N 3M5, Canada

ABSTRACT

During investigations of potential child and elder abuse, clinicians and forensic practitioners are often asked to offer opinions about the age of a bruise. A commonality between existing methods of bruise aging is analysis of bruise color or estimation of chromophore concentration. Relative chromophore concentration is an underlying factor that determines bruise color. We investigate a method of chromophore concentration estimation that can be employed in a handheld imaging spectrometer with a small number of wavelengths. The method, based on absorbance properties defined by Beer-Lambert's law, allows estimation of differential chromophore concentration between bruised and normal skin. Absorption coefficient data for each chromophore are required to make the estimation. Two different sources of this data are used in the analysis- generated using Independent Component Analysis and taken from published values. Differential concentration values over time, generated using both sources, show correlation to published models of bruise color change over time and total chromophore concentration over time.

Keywords: Methods: feature extraction, Modalities: optical imaging, Diagnostic Task: detection

1. INTRODUCTION

We are motivated in this effort by a demonstrated need to improve the identification of bruises from elder and child abuse. During investigations of potential child and elder abuse, clinicians and forensic practitioners are often asked to offer opinions about the extent and age of a bruise. Visual inspection in vivo and photography of bruises are two conventional methods employed in clinical practice[1, 2]. However they are qualitative, subjective, inaccurate and hence unreliable. Spectroscopy has emerged in the field and has shown improvements in the reliability of bruise aging[3, 4].

The spectral response of the normal and diseased skin can be analyzed for hidden variables such as erythema index, oxygen saturation, dermal blood volume, and concentration of various chromophores in the skin[3-7]. Point spectrometers measure spectral response as a single point on the body. By taking multiple measurements in a localized area, one can create a distribution map of the chromophores. However, in clinical practice, point spectroscopy may be too time consuming and tedious to create a distribution map of the chromophore concentrations[8]. For this reason, a system that can capture an area of tissue is more clinically appropriate.

The distribution of chromophores is indicative of important information about the bruise, such as source of trauma and age of the bruise[3, 9]. Recently, research has been done using spectrophotometry to create distribution maps of chromophores in skin. Spectrophotometers yield images in which the spectral response at each pixel pertains mainly to the skin directly underneath that pixel. With these images, spectral analysis can be applied over a broad area of tissue with a single measurement. Vogel et al have used a 4 wavelength spectral imaging system to create chromophore concentration maps of Kaposi-Sarcoma lesions[6]. This work demonstrated the ability to show oxygen saturation and blood volume. Tsumura et al have demonstrated the ability to create hemoglobin and melanin maps from color photos of human skin[10]. Work by Sprigle et al has shown the capability to create contrast-enhanced images of erythematic skin[11], which is closely related to chromophore concentration maps.

Existing methods of bruise aging share a commonality, the analysis of bruise color or chromophore concentration. Changes in bruise color are attributed to the breakdown of hemoglobin into by-products which include biliverdin, bilirubin, and hemosiderin[1, 3]. Each of these chromophores has a unique spectral response. As hemorrhaging ceases and hemoglobin breakdown commences, relative chromophore concentrations change. This results in a spectral response that influences observed bruise color. There are however other factors that influence bruise color such as melanin concentration and skin thickness.

The goal of our project is development of a point-of-care imaging device for the visual enhancement and aging of bruises. We have employed an 11-wavelength multi-spectral imaging system to investigate methods for enhancing and aging bruises. Using our system we collected images of clinical bruises for analysis. We chose to investigate the breadth of clinical bruises rather than induced bruises. This presented us with bruises of different etiologies and location than we would see in induced bruises.

In this paper, we investigate a method for bruise aging, specifically, chromophore concentration estimation that can be employed in a handheld imaging spectrometer with a small number of wavelengths. The method is capable of giving differential chromophore concentration estimates without measuring incident light. Using the method along with a model of differential concentration versus bruise age, we hope to be able to estimate the age of a bruise.

2. METHODS

Residents of an extended care facility and students and staff of our lab were recruited for the study. Ages ranged from 19-86. Subjects were divided into two groups consisting of subjects younger than 65 years of age and subjects at least 65 years of age. We chose this criterion to be consistent with work by Langlois and Gresham, which demonstrated a significant difference in the development rate of yellow between the two groups[2]. Subjects of the younger group had much more consistent bruising patterns and time to resolution than did the subjects of the elder group. Because the accuracy of the reported bruise onset date was deemed unreliable within the elder group, only bruises from subjects younger than 65 years of age are analyzed in this paper. The analyzed dataset consists of 58 images from 12 bruises.

Most bruises were imaged on several different occasions after discoloration was reported. Bruise location was often marked with surgical marker so that we could image the same spot on different occasions. For most of the bruises, the first images were taken after the first twenty-four hours. Bruises occurred within everyday life (i.e. we did not induce any of the bruises), which meant we were unable to image the bruises until visible discoloration was perceived. This also meant the etiology and location were uncontrolled. Some subjects had multiple bruises imaged during the course of this study.

2.1 Multi-spectral imaging system

A rotating filter wheel style imaging system collected data for this research (Figure 1). The imaging system was mounted on a tripod and could be transported to location of the subject. The sensor for the system was a Unibrain Fire-i™ CCD camera (Unibrain, S.A., resolution 640x480pixels, 8-bit grey-scale per pixel). Located in front of the camera was the rotating motorized filter wheel, which could accommodate 12 filters. The system was fit with 11 bandpass filters (FWHM: 10nm~40nm) with center wavelengths in the range of 370-970nm. One filter position was left open to get a wideband reference image. The filters targeted the absorption peaks and isobestic points of the primary chromophores of blood and skin. Multispectral images were acquired by sequentially changing filters in front of the camera lens resulting in a series of images – an image cube.

Figure 1: The spectral imaging system. The filter wheel and illumination are visible. The camera is located behind the left side of the filter wheel.

A rectangular arrangement of four 40-watt halogen bulbs provided illumination. The camera was centered in the arrangement. This lighting system provided adequate lighting in the 415-970 nm wavelength range; however the power output at wavelengths below 415nm was not sufficient. Measurements at wavelengths below 415 were not used in this study because the signal to noise ratio was too low.

The illumination system had a non-uniform spectral power distribution across the wavelengths of interest, thus the gain and shutter speed of the camera were adjusted on an individual wavelength basis. Gain and shutter speed were also adjusted on a subject basis, with the intention of maximizing the dynamic range in the resultant images. The system was controlled using custom in house software written in LabVIEW (National Instruments Corp. Austin, TX). Information about the bruise such as onset date, location, subject age, gender, and skin color were recorded by the software. For more information about the imaging procedure see our previous publication[12].

2.2 Image preprocessing

Multispectral images were preprocessed before analysis. The first step was cropping the image to include only areas of skin surrounding the bruise. This promoted good curvature correction because discontinuous surfaces were excluded from curve fitting. The second step was correction of shading due to surface curvature. This was done by fitting a quadratic surface to the cropped intensity image. The fitted surface was normalized so that its maximum value is one. The cropped image was then corrected for shading artifacts by dividing by the fitted surface.

We fit a quadratic surface to the cropped image using the *lsqcurvefit* function in MATLAB's Optimization Toolbox (The Mathworks, Inc.). The use of a quadric allowed us to fit second order curvature and was robust to images where the main axes of curvature did not align with the x- and y-axes of the image. This method of curve fitting required us to exclude any bruise pixels from the procedure. We hand selected a rectangular region of pixels that fully encompassed the bruise. These pixels were excluded from the fitting.

In some situations it may be more appropriate to reduce the human input in processing or to maximize the number of pixels used for fitting. For this we have devised a minimum entropy curvature correction technique based on Likar et al [13]; however this method is not used in this paper.

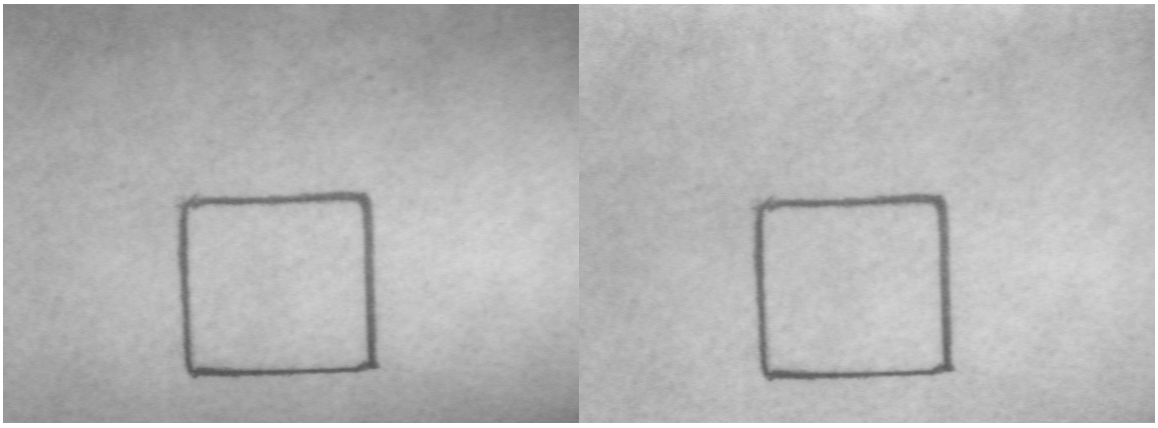

Figure 2: Cropped image (left) versus curvature corrected cropped image (right). The curvature correction procedure was able to remove the first and second order shading artifacts. Higher order shading artifacts are still apparent in the curvature image.

Region-of-interest (ROI) selection was also included in the preprocessing stage. A rectangular region, B, of pixels in the bruised skin was selected as the Bruise ROI. Four rectangular regions of adjacent normal skin, N_{1-4}, were selected as the Normal Skin ROI. For this work, values were averaged over B and N, thus the native registration accuracy of the multispectral image sufficed allowing us to omit any additional registration. For creation of chromophore maps, registration with sub-pixel accuracy is required. This has proved to be somewhat difficult with the current imaging system due to slight subject movements and optical aberrations. Concurrent research has developed technology for capturing a 4-wavelength spectral image simultaneously[14].

2.3 Analysis

We previously introduced the notion of normalized bruise reflectance (NBR) values[12]. NBR values are calculated by dividing the mean pixel value of B by the mean pixel value of N. According to Beer-Lambert's law, the negative log of the calculated NBR is equal to the absorbance difference, A_d, between the bruised skin and normal skin (eq 1).

$$A_d = A_b - A_n = -\log(NBR) \tag{1}$$

The Beer-Lambert law asserts that total absorbance is the sum of absorbance from each of the constituent absorbers (eq 2). Absorbance due to each absorber is the product of the absorption coefficient α of the absorber, the path length (l) the light travels through the absorber, and the concentration (c) of the absorber.

$$A = \sum\nolimits_i \alpha_i l_i c_i \tag{2}$$

Absorbance, absorption coefficient, and path length are all a function of wavelength. We can state equation 2 formally as equation 3. For the rest of this paper we will use the syntax of equations 2 and 3 interchangeably.

$$A(\lambda) = \sum\nolimits_i \alpha_i(\lambda) l_i(\lambda) c_i \tag{3}$$

We employ a simple skin model in which the chromophores are uniformly distributed within each layer of skin. This is not an uncommon assumption[6]. We also assume that the mean path length does not change as a function of chromophore concentration, thus we have a constant path length between normal skin and bruised skin. Skin thickness varies as a function of body site, however we will also assume that because of the proximity of B and N, the skin thickness between does not vary. Using this model, we put A_d in terms of the concentration difference of each absorber in eq 4.

$$A_d = A_b - A_n = \sum\nolimits_i \alpha_i l_i (c_{ib} - c_{in}) = \sum\nolimits_i \alpha_i l_i c_{id} \tag{4}$$

c_{ib} is the concentration of chromophore I in the bruised skin. c_{in} is the concentration of chromophore i in normal skin. c_{id} is the difference in concentration of chromophore i between bruised and normal skin.

2.3.1 Calculating differential concentration levels

To calculate differential concentration levels, we set up a system of equations X=MS. X contains the differential absorption values for each wavelength, λ, for each measurement in our data set; this is our observed data. Columns of X correspond to wavelengths, λ_1 through λ_{11}. Rows of X correspond to different measurements (spectral images) I_1 through I_m, each of which represents a bruise on a subject at a certain age.

$$X = \begin{bmatrix} A_{d,I_1}(\lambda_1) & \cdots & A_{d,I_1}(\lambda_{11}) \\ \vdots & \ddots & \vdots \\ A_{d,I_m}(\lambda_1) & \cdots & A_{d,I_m}(\lambda_{11}) \end{bmatrix} \tag{5}$$

S contains the values of the absorption coefficients for each absorber at each wavelength. These are our source signals. As in X, columns of S correspond to λ_1 through λ_{11}. Rows of S correspond to the different absorbers.

$$S = \begin{bmatrix} \alpha_1(\lambda_1) & \cdots & \alpha_1(\lambda_{11}) \\ \vdots & \ddots & \vdots \\ \alpha_n(\lambda_1) & \cdots & \alpha_n(\lambda_{11}) \end{bmatrix} \tag{6}$$

M is the mixing matrix, and demonstrates how the source signals mix to get X. Contextually, M represents the differential concentration and path length of each of the chromophores for each measurement. Since we are not separating the differential concentration and path length values in this work, we will just take the contents of M as differential concentration. By setting up a system of equations (eq 7), we can solve for M.

$$\begin{bmatrix} A_{d,I_1}(\lambda_1) & \cdots & A_{d,I_1}(\lambda_{11}) \\ \vdots & \ddots & \vdots \\ A_{d,I_m}(\lambda_1) & \cdots & A_{d,I_m}(\lambda_{11}) \end{bmatrix} = \begin{bmatrix} (cl)_{1,I_1} & \cdots & (cl)_{n,I_1} \\ \vdots & \ddots & \vdots \\ (cl)_{1,I_m} & \cdots & (cl)_{n,I_m} \end{bmatrix} * \begin{bmatrix} \alpha_1(\lambda_1) & \cdots & \alpha_1(\lambda_{11}) \\ \vdots & \ddots & \vdots \\ \alpha_n(\lambda_1) & \cdots & \alpha_n(\lambda_{11}) \end{bmatrix} \tag{7}$$

2.3.2 Source signals

We generate S in two different ways. This must be done before we can solve for M. The first way is by independent component analysis (ICA), using a method similar to Polder[15]. ICA is a form of source signal separation that estimates source signals and the mixing matrix given the observed signals. In general, the discovered independent components can be interpreted as underlying causes of observations, especially when one believes that: (1) observed features are generated by the interaction of a set of independent hidden random variables, and (2) these hidden variables are likely to be kurtotic (*i.e.* each variable is discriminative and sparse). ICA has-been used in a variety of blind source separation problems including audio source separation[16], image segmentation[17], and fMRI of the brain[18]. In this work we used a highly efficient version of the ICA algorithm, FastICA[19]. FastICA can be called with numerous parameterizations. We used a deflation estimate approach with the g(u)=u^3 "pow3" contrast function. Convergence was estimated using epsilon (0.0001) threshold difference in the separating matrix.

The other method of generating S is the use of published absorption coefficient curves[4, 20]. We generated S with absorption coefficient data for deoxygenated-hemoglobin (Hb), oxygenated-hemoglobin (HbO_2), and bilirubin. We also generated S with absorption coefficient data for just Hb and bilirubin. Work by Randeberg suggests that Hb and bilirubin are the two chromophores that are most important in bruise aging[3].

The method of calculating M is dependent on how S is generated. When FastICA generates S (S-ICA), M is generated simultaneously. When using published absorption coefficient data for S (S-trio and S-sansHbO_2), we generate M by finding the least squares solution with MATLAB.

3. RESULTS AND DISCUSSION

3.1 Sources from ICA

Prior to estimating the independent components (ICs), FastICA will apply principle component analysis (PCA) to reduce the dimensionality of the data. The number of dimensions reduced to is user defined; we specified it to be 3 in order to fit a model where the absorbers were Hb, HbO_2, and bilirubin. These first 3 eigenvectors account for 88.9% percent of total variance in the data. Figure 3 shows the variance accounted for by the top k eigenvectors. The shape of this curve indicates that there may be more than 3 natural dimensions in the data; however the use of more dimensions does not fit our physiological model.

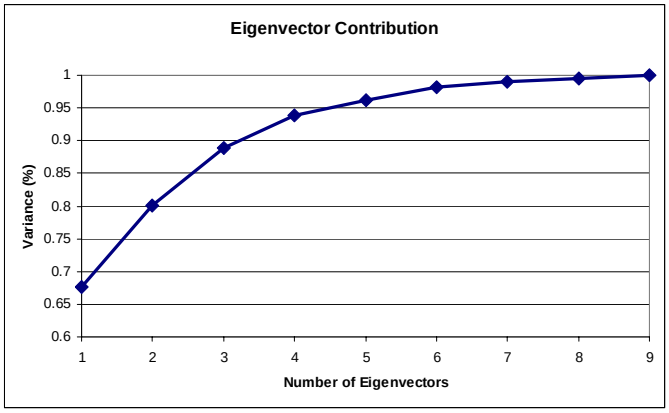

Figure 3: Total variance in the data set represented in the top k eigenvectors.

The number of ICs produced by FastICA is also user defined. Again, we specified 3 ICs to fit our physiological model. The resulting ICs are plotted with the published normalized absorption coefficient curves in Figure 4. It should be noted that the curves are normalized to 1, with the exception of the Hb curve which is normalize by the same factor as the HbO_2 curve to preserve the isobestic points. Curves are normalized to show shape rather than absolute value because ICA is insensitive to scaling. For that same reason, curves may be flipped over the x-axis.

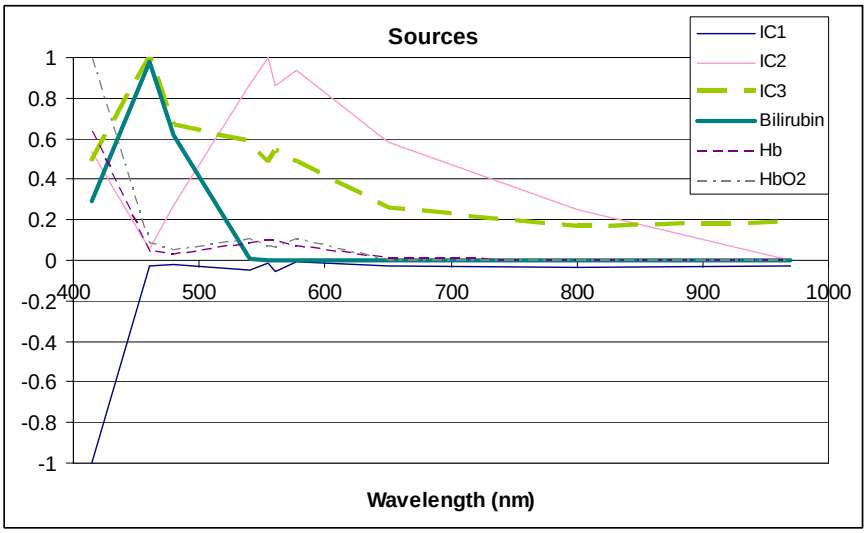

Figure 4: Source signals (IC1, IC2, IC3) estimated by ICA plotted with normalized absorption coefficients.

The ICs plotted in Figure 4 are results of FastICA run on the dataset. However, FastICA did not always converge on the same result. This is in part due to the fact that the algorithm begins with a randomize estimate of the unmixing matrix. Depending on the initial estimate, FastICA can produce different results. In the case of the results presented in Figure 4, all of them seem to have a ``notch" feature between 540 and 577, which is characteristic of the HbO_2 curve. This seems to indicate a residual source that is not

separated, but rather diffused among each of the three sources (i.e. there seem to be more than three sources in the data). A physiological model for bruise aging with more than three sources may factor in biliverdin and hemosiderin.

Estimates of the differential concentration given in the mixing matrix M produced by FastICA are plotted in Figure 5. This graph shows data for all subjects. There is a high amount of variation in this data, which indicates a weakness of creating an aging model by correlating these results with the ages of naturally acquired bruises.

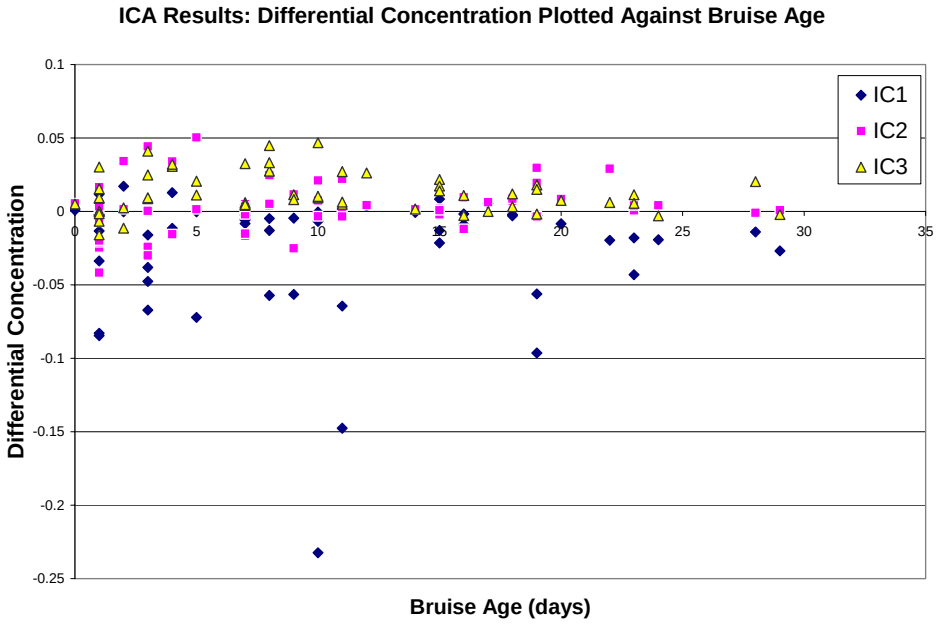

Figure 5: Differential concentration for the three estimated path length versus age of the bruise. All subjects.

There are some patterns that are visible in the plot. The values exhibit high variance around the lower bruise age. As bruise age increases the variance appears to shrink and the concentration tends to zero. High variance in the younger bruises can partially be accounted for by varying etiology and location of the bruises. IC3 appears to exhibit concentration change characteristic of bilirubin. The concentration rises for the first few days and then begins to fall after approximately day 10. The peak concentration of bilirubin is said to occur between day 6 and day 12, which almost matches with our data. Furthermore, the shape of IC3 (Figure 4) most closely matches the absorption coefficient curve of bilirubin.

3.2 Sources from published absorption coefficients

Estimation of M using published absorption coefficient curves was done for two different sets S-trio and S-sansHbO_2. S-trio was composed of absorption coefficients for Hb, HbO_2, and bilirubin. S-sansHbO_2 was composed of Hb and bilirubin. HbO_2 was left out of the second set because we do not expect to see much extravascular HbO_2 after the initial stages of bleeding, and most of our data was collected 24 hours or more after trauma. Melanin is not included in either of the sets because our skin model suggests that there will be no difference in melanin concentration or path length between the bruised and normal skin.

The differential concentration values for all subjects (from M) are plotted as a function of bruise age for S-sansHbO_2 (Figure 6). Figure 7 contains this data plotted for four individual bruises: A, B, C, and D.

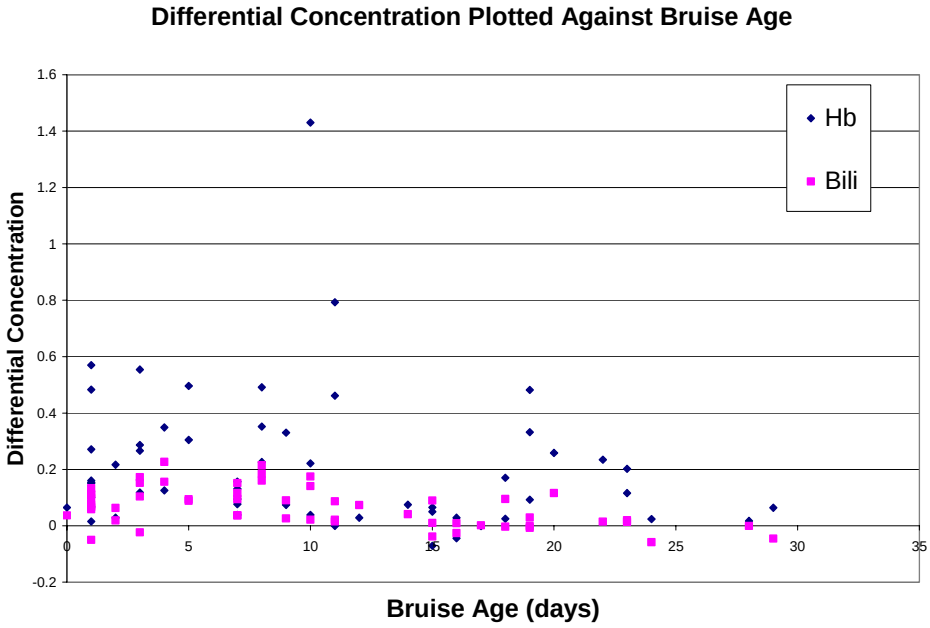

Figure 6: Differential concentration for S-sansHbO$_2$, plotted for all bruises. As age increases, differential concentration changes eventually tending back to zero as the bruise resolves.

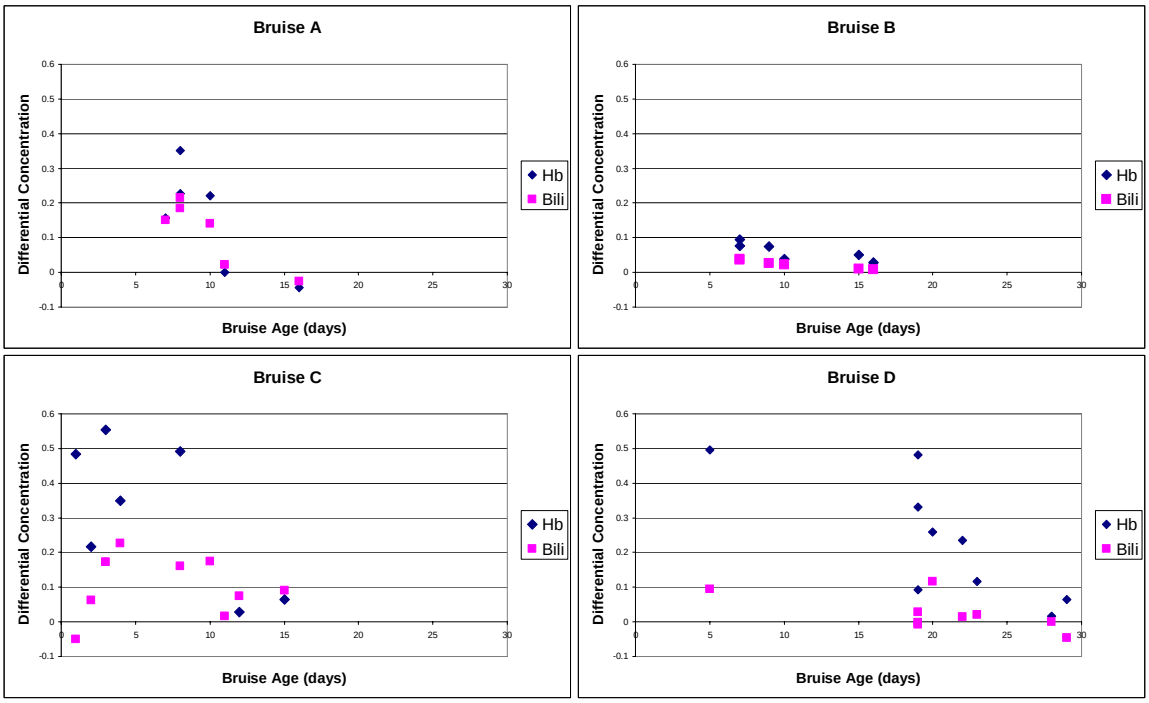

Figure 7: Differential concentration and path length for S-sansHbO$_2$. Bruise C has 2 data points that fall out of the range of the chart.

The differential concentration plot for all bruises shows high variance, but it also shows general trends. Day 1 (24-48hours after the trauma event) was the first day the majority of the bruises were imaged. We see a spread of values for differential concentration of Hb for the first few days. Then, with the exception of a few outliers, the differential concentration tends to zero at the end of the second week. According to Langlois, bleeding may continue for 24-48 hours after the trauma event[2]. This would result in a maximal concentration of Hb and HbO2 in that period, which agrees with what we see. Degradation of Hb occurs

slowly over a matter of days. Bilirubin, a breakdown product of Hb, begins to form several hours after trauma. Yellow color, produced by bilirubin, has been reported to peak in the range of 6 to 12 days after trauma[1, 2]. The differential concentration of bilirubin appears to increase until it peaks between day 4 and 8, and then it decreases with time. Strangely, the data also shows a spike in hemoglobin concentration around day 19. This is unexplained by bruising models but the spike appears to be primarily the result of a single bruise. The presence of bruising after two weeks contrasts the published aging models, which define resolution after 2 weeks. The bruises we saw that lasted longer than two weeks may be outliers, but they also demonstrate the variations in clinical bruising.

Data for the individual bruises (Figure 7) does not clearly demonstrate the trends in shown by the complete group. For Bruise A, the differential concentration of Hb and bilirubin are both high at day 7, the first day of imaging. The concentration of both chromophores drops to zero as the bruise age approaches two weeks. Bruise B exhibits the same pattern as bruise A, although overall the concentration levels are lower on B. Bruise A and B are from the same subject which may contribute to the similar aging pattern. Bruise C was imaged over most of its lifetime. It has high a differential concentration of bilirubin from 3 to 10 days and lower concentration outside this period. The differential concentration of Hb in this bruise exhibits strange patterns which do not agree with bruising models. Bruise D exhibits an over all trend of concentration levels falling to zero, yet it has some abnormal features. This bruise lasted almost one month before resolution, which exceeds the published duration of bruising. On day 19, the bruise was imaged three times with slight changes in the imaging setup. The variation in calculated differential Hb concentration levels for that day, demonstrates the sensitivity of this method to changes in data collection and processing. It is also interesting to note that the calculated bilirubin concentration does not vary to the same extent as Hb.

When we solve for differential concentration using the three source model, S-trio, different results appear. The differential bilirubin concentration keeps a similar shape as with S-sansHbO_2 but the real difference is in the concentration levels of Hb. Differential concentration of Hb as a function of bruise age keeps a similar shape, but the values are a magnitude of order higher than with S-sansHbO_2. The concentration of HbO_2 is on the same order of magnitude as Hb, but the values are negative. This might suggest that the absolute levels of HbO_2 are lower in bruised skin than in normal skin, although there is no other evidence to support this.

4. CONCLUSION

A technique for estimating differential concentrations of bruise chromophores was presented in this paper. The technique can be employed in a multispectral imaging system employing a small number of wavelengths. We used 10 wavelengths in our analysis, but the technique would allow use of as few wavelengths as there are chromophores. Using more wavelengths results in an over determined system.

Differential concentration as a function of bruise age appears to correlate with published bruise aging models. However, the high amount of variance in conjunction with the small data set used does not bode well for creating an aging model from this data.

We have refined our data collection system since the end of data collection for this study. These changes include addition of an achromatic lens, higher quality filters, and a cross-polarization illumination system to eliminate specular reflection from our captured images. We hope to collect a larger dataset with this system for later analysis.

The bruises within this data set occurred naturally so varied in location, cause and size and demonstrated high variability. We will continue to work over the breadth of clinical bruises to capture the different etiologies and location of bruising. This variability needs to be accounted for when generating aging models.

We also hope to improve the analysis in future work. Application of a light path length model and a more advanced skin model may improve and give more meaning to the results. Models which depend on subject skin thickness may require extra instrumentation such as ultrasound for skin thickness measurement. Additionally, ultrasound has potential for characterization and aging of bruised tissue.

This work also demonstrates the use of ICA for human bruise characterization. Although the application of ICA in this study did not give us extraordinary results, it should not be taken as an indication of ICA's applicability in this field. Polder et al has already demonstrated the ability to recover the absorbance

coefficients of the two main chromophores in tomatoes[15]. Tsumura has demonstrated the ability to extract melanin and hemoglobin distribution maps in human skin using ICA[10]. Some factors that may have contribute to the results we saw may be noise or presence of another source. Also, better results may be obtained through tuning the parameters of FastICA.

REFERENCES

1. Dimitrova, T., et al. *Qualitative visual image analysis of bruise age determination: A survey*. in *Proc of the 28th IEEE EMBS Annual International Conference*. 2006. New York City, USA.
2. Langlois, N.E. and G.A. Gresham, *The ageing of bruises: a review and study of the color changes with time.* Forensic Sci Int., 1991. **50**: p. 227-238.
3. Randeberg, L.L., et al., *A novel approach to age determination of traumatic injuries by reflectance spectroscopy*. Lasers in Surgery and Medicine, 2006. **38**(4): p. 277-289.
4. Randeberg, L.L., *Diagnostic applications of diffuse reflectance spectroscopy*, in *Department of Electronics and Telecommunications*. 2005, Norwegian University of Science and Technology: Trondheim. p. 62.
5. Nishidate, I., Y. Aizu, and H. Mishina, *Estimation of Absorbing Components in a Local Layer Embedded in the Turbid Media on the Basis of Visible to Near- Infrared (VIS-NIR) Reflectance Spectra.* Optical Review, 2003. **10**(5): p. 427-435.
6. Vogel, A., et al., *Using noninvasive multispectral imaging to quantitatively assess tissue vasculature.* J Biomed Opt, 2007. **12**(5): p. 617-36.
7. Sowa, M.G., et al., *Spectroscopic assessment of cutaneous hemodynamics in the presence of high epidermal melanin concentration.* Clin Chim Acta, 2002. **317**(1-2): p. 203-12.
8. Stamatas, G.N., C.J. Balas, and N. Kollias. *Hyperspectral image acquisition and analysis of skin*. in *Proceedings of SPIE: Spectral Imaging: Instrumentation, Applications, and Analysis II*. 2003: SPIE.
9. Randeberg, L.L., et al. *Hyperspectral imaging of bruised skin*. in *Proc. SPIE Vol. 6078: Photonic Therapeutics and Diagnostics II*. 2006.
10. Tsumura, N., et al. *Mapping pigmentation in human skin by multivisible-spectral imaging by inverse optical scattering technique*. in *IS&T/ SID's 8th Color Imaging Conference, Color Science, Systems*. 2000.
11. Sprigle, S., L.W. Zhang, and M. Duckworth, *Detection of Skin Erythema in Darkly Pigmented Skin Using Multispectral Images.* Advances in Skin and Wound Care, 2008. **In Press.**
12. Sprigle, S., et al. *Multispectral image analysis of bruise age*. in *Medical Imaging 2007: Computer-Aided Diagnosis.* 2007. San Diego, CA, USA: SPIE.
13. Likar, B., et al., *Retrospective shading correction based on entropy minimization.* J Microsc, 2000. **197**(Pt 3): p. 285-95.
14. Kong, L., et al. *Handheld erythema and bruise detector*. in *Medical Imaging*. 2008. San Diego, CA, USA: SPIE.
15. Polder, G., G.W.A.M. van-der-Heijden, and I.T. Young, *Tomoto sorting using independent component analysis on spectral images.* Real-Time Imaging, 2003. **9**: p. 253-259.
16. Bell, A.J. and T.J. Sejnowski, *An information maximization approach to blind separation and blind deconvolution to blind source separation and blind deconvolution.* Neural Computation, 1995. **7**(6): p. 1129-1159.
17. Bell, A.J. and T.J. Sejnowski, *The independent components of natural scenes are edge filters.* Vision Research, 1997. **37**: p. 3327-3338.
18. McKeown, M.J., et al., *Analysis of fMRI data by blind separation into independent spatial components.* Human Brain Mapping, 1998. **6**: p. 160-188.
19. Hyvarinen, A., *Independent component analysis in the presence of gaussian noise by maximizing joint likelihood.* Neurocomputing, 1998. **22**: p. 49-67.
20. Zijlstra, W.G., A. Buursma, and O.W.v. Assendelft, *Visible and Near Infrared Absorption Spectra of Human and Animal Haemoglobin: Determination and Application.* 2000, Utrecht: VSP.